Available online at www.sciencedirect.com
ScienceDirect
Ceramics International 37 (2011) 2603–2608
CERAMICS INTERNATIONAL
www.elsevier.com/locate/ceramint

Structural and optical properties of Ho_2TeO_6 micro-crystals embedded in tellurite matrix

C. Joshi, Y. Dwivedi, S.B. Rai *

Laser & Spectroscopy Laboratory, Department of Physics, Banaras Hindu University, Varanasi 221005, India

Received 5 February 2011; received in revised form 2 April 2011; accepted 5 April 2011
Available online 13 April 2011

Abstract

In the present work, Ho^{3+} doped tellurite glasses and glass ceramics have been explored. Micro-sized Ho_2TeO_6 crystals have been successfully prepared in TeO_2 matrix using two step heat treatment method. Structural, thermal and optical properties have been investigated using different characterization techniques. Variations in above mentioned properties were observed to improve when these crystals grew in TeO_2 matrix. We have reported several anti-Stokes and Stokes emissions extended from UV to NIR region on excitation with 532 and 976 nm laser radiations. The unique structure of Ho_2TeO_6 crystal was expected to play a crucial role in enhancement of the optical properties of glass ceramics.

PACS : 74.25 Gz; 42.70 Hj; 73.61 Jc; 76.30 Kg; 42.70 Ce

Keywords: D. Glass ceramic; Tellurite glass; Anti-Stoke's emission; FTIR analysis; Upconversion

1. Introduction

Rare earth (RE) ion activated materials remain a hot topic of investigation as these materials have been extensively used in various applications viz. high performance magnet, luminescent devises, laser materials, telecommunications, biomedical and many others [1–4]. Peculiar electronic, optical and chemical properties of RE ions are seen from their 4f electrons in different environments. One of the most discussed properties of RE ions is the upconversion process. Because of the long lived radiative levels, upconversion emissions are frequently realized and utilized to simulate different colors. The optical properties of the RE ions are function of the chemical composition and local environment around the ions. Recently, glasses dispersed with nano-crystals gained the special attention because of their prospective use as a promising host for RE ions [5–9]. These glass ceramics are two phase systems consisting of a base glass within which crystals are grown by controlled nucleation of the crystal phase and subsequent crystallization in a precursor glass by thermal process. These lattices are advantageous as they have higher mechanical and chemical stability and have low phonon frequencies.

Among rare earth ions, Ho^{3+} ion has been extensively investigated owing to the observation of laser action in infrared and visible regions [10,11]. It is one of the important active ions applied to upconversion luminescence because of its favorable energy level structure. It has a high lying green emitting level ($^5F_4$, $^5S_2$) and metastable levels ($^5I_7$ and $^5I_6$) from where efficient infrared excited state absorption (ESA) processes take place. Also, many non-radiative energy transfer processes such as cross-relaxation and upconversion can help in building upconverted population.

Tellurite glasses [12,13] are of technical interest because of their low melting temperatures, lower phonon vibrations (600–800 cm^{-1}) and non-hygroscopic properties. Besides these characteristics, tellurite glasses have many other superiorities over other glassy systems such as their high refractive index [14], anomalous partial dispersion in the visible region, high third-order non-linear susceptibility [15,16], good host for RE ions [17] and optical amplifying properties [18] as well as good transmittance in the near infrared region (NIR) [19]. In many cases, these properties are combined with good chemical and crystallization properties

* Corresponding author. Tel.: +91 542 230 7308; fax: +91 542 236 9889.
E-mail address: sbrai49@yahoo.co.in (S.B. Rai).

0272-8842/$36.00
doi:10.1016/j.ceramint.2011.04.005

[20] to make it as one of the suitable hosts for such type of applications.

In the present work, for the glass preparation, we have taken TeO_2 as network former and Li_2CO_3 and ZnF_2 as network modifiers. Introducing zinc fluoride (ZnF_2) to this glass matrix restricts the lattice vibration considerably. It acts as modifier as well. Fluorine ions break the Te–O bonds while Zn^{2+} ions occupy interstitial positions to form Zn–O–Te linkages because of the close ionic radii of Te^{4+} (0.7 Å) and Zn^{2+} (0.74 Å) ions [21]. Also, addition of ZnF_2 into TeO_2 glass matrices results in lowering its viscosity [22].

In this paper, we report a study on the optical, thermal and structural properties of rare earth ion Ho^{3+} doped oxyfluoro tellurite glasses. We have also described the influence of zinc fluoride on the luminescence and upconversion processes in tellurite glasses and glass ceramics.

2. Experimental

Glass samples were prepared using these chemicals as starting materials according to following compositions in mol.%:

$$74\,TeO_2 + 25\,Li_2CO_3 + 1\,Ho_2O_3, \quad \text{referred as Li : } TeO_2, \text{ and}$$

$$69\,TeO_2 + 25\,Li_2CO_3 + 5\,ZnF_2 + 1\,Ho_2O_3, \quad \text{referred as Zn : Li : } TeO_2$$

The conventional melt-quench method has been used for the preparation of glass samples. The concentration of Ho^{3+} was kept below to the concentration quenching limit. All powder materials used were of analytical grade. The well mixed starting materials were first melted at 900 °C in a platinum crucible for 30 min in an electric furnace. The molten mixture (free from air bubbles) was quenched by squeezing it into a rectangular steel cast preheated to 200 °C. The glasses were then cooled to room temperature gradually. The given compositions of all samples were optimized according to their maximum luminescent intensities. The as-prepared glass samples were further heated to 390 °C for 2 h to obtain their ceramics.

In order to determine the characteristic glass transition temperature, crystallization temperature, and melting temperature, differential temperature analysis (DTA) of the glass samples was carried out by a Rigaku Thermoplus analyzer (DSC8270). The crystalline structure of the glass ceramic samples was verified by the powder X-ray diffraction (XRD) using CuKα radiation (1.5406 Å) with nickel filter. The crystallite size was calculated using Scherrer relation. The UV–vis–NIR absorption spectra were obtained at room temperature using a Shimadzu UV 1201 spectrophotometer. Perkin Elmer Spectrum RX1 was used to record the FTIR absorption spectra of the samples. The up and down-conversion emission spectra were recorded using 976 nm wavelength from a diode laser and 532 nm wavelength from Nd:YAG laser as excitation sources. An iHR320, Horiba Jobin Yvon, spectrometer was used to detect the fluorescence signal.

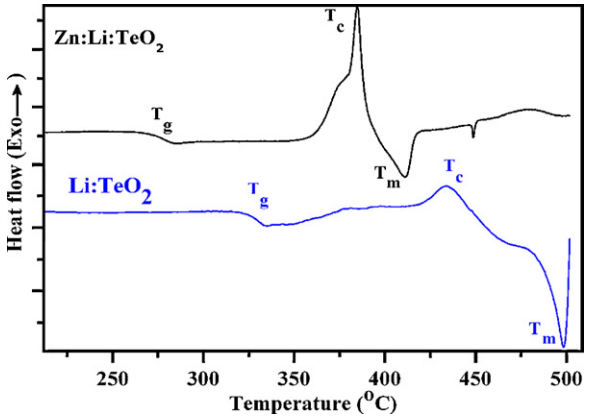

Fig. 1. Differential thermal analysis curves of $Li:TeO_2$ and $Zn:Li:TeO_2$ glass samples.

3. Results and discussion

3.1. Thermal characterization

DTA curves of $Li:TeO_2$ and $Zn:Li:TeO_2$ glasses are shown in Fig. 1. DTA scan of $Li:TeO_2$ exhibits an endothermic hump corresponding to the glass transition temperature (T_g) at 322 °C which is followed by three exothermic peaks corresponding to crystallization temperature (T_c) at 382 °C, 397 °C and 433 °C and another endothermic event corresponding to the melting temperature (T_m) at 499 °C. The two exothermic peaks at 382 °C and 397 °C are due to the co-existence of oxide phases of tellurite glass (γ-TeO_3 and α-TeO_3 polymorphics), while the stable α-TeO_3 phase appears at 433 °C temperature. The lack of sharp endothermic and exothermic peaks in the DTA curves clearly indicates the formation of homogeneous glass. On the contrary of $Li:TeO_2$ glass, the glass transition temperature of $Zn:Li:TeO_2$ glass reduces to 271 °C and a sharp crystallization peak at 385 °C overlying a broad peak centered at 375 °C is observed, which is entirely different compared to $Li:TeO_2$ glass. The endothermic process corresponding to the melting point temperature (T_m) is observed at 412 °C. The change in T_g clearly reflects that how ZnF_2 affects the structure and gets arranged in the glass. A decrease in glass transition temperature implies a decrease in the rigidity of the network.

The glass stability can be determined qualitatively by a difference of T_c and T_g, i.e. ($T_c - T_g$) and its larger value leads to high thermal stability of the glass. Its value is found to be 111 °C in case of $Li:TeO_2$ glass while it is 114 °C in case of $Zn:Li:TeO_2$ glass. Another relevant parameter called Hruby's parameter (H_R) has been calculated using the relation

$$H_R = \frac{T_c - T_g}{T_m - T_c}$$

where the terms have their usual meaning. H_R gives information about the stability of the glass against devitrification and its value is found 1.68 in $Li:TeO_2$ glass while it is 4.22 in $Zn:Li:TeO_2$ glass.

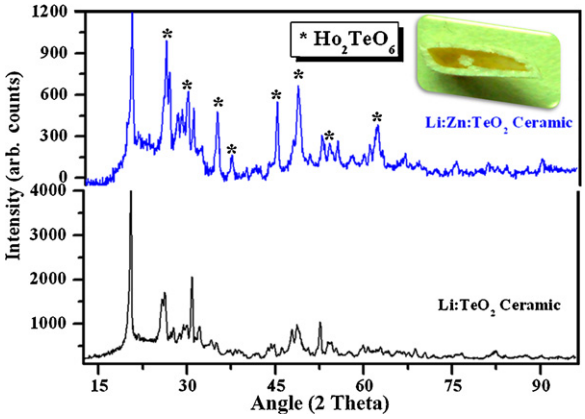

Fig. 2. X-ray diffraction pattern of $LiTeO_2$ and $Zn:Li:TeO_2$ glass ceramics (390 °C/2 h). Cross sectional view of the surface crystallized glass ceramic sample is given in inset.

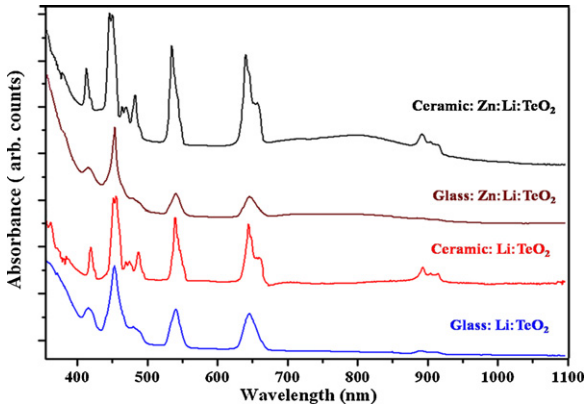

Fig. 3. UV–NIR absorption spectra of the $Li:TeO_2$ and $Zn:Li:TeO_2$ glass and glass ceramic samples.

3.2. Phase characterization

The XRD patterns of the crushed powders of two glass ceramic (heated at 390 °C for 2 h) samples $Li:TeO_2$ and $Zn:Li:TeO_2$ are shown in Fig. 2. The several sharp peaks overlying the humps are the clear evidence of the formation of tiny crystallites in the residual glass matrices. The XRD pattern of the $Li:TeO_2$ glass ceramic sample contains only TeO_2 phase, however, in case of $Zn:Li:TeO_2$ glass ceramic sample, intensities of the TeO_2 phase reduce and at the same time a few new peaks also appear. The new Bragg peaks are assigned to the mixed phases of Ho_2TeO_6 (holmium oxotellurates: JCPDS data file 40-0330) and TeO_2 crystals in major and minor proportions, respectively. Generally, Ho_2TeO_6 phase starts growing after heating at a higher temperature (900 °C) for 23 h continuously [23] but in the presence of ZnF_2, this phase appears at a much lower temperature 390 °C after heating only for 2 h. It can be concluded that the presence of small amount of Zn in the $Li:TeO_2$ lattice promotes the formation of Ho_2TeO_6 phase. M_2TeO_6 (M = RE ions) type of crystals consists of two structures, the orthorhombic ($P2_12_12_1$) and the trigonal (P_32_1). In both type of structures, the Te^{6+} cations exhibit sixfold oxygen surroundings in form of isolated $[TeO_6]^{6-}$ octahedral [24]. The sizes of these crystals are determined using Debye–Scherrer formula

$$D_{hkl} = \frac{K\lambda}{\beta \cos\theta}$$

where λ is the wavelength of incident X rays (~1.54056 Å), θ is the angle of diffraction, β is the full width at half maximum (FWHM) of the diffraction peak and the constant $K = 0.90$. It gives average size of the crystals about 300 nm.

It was observed that the crystallization starts from the surface. It has been reported that if the chemical composition of a glass phase is nonstoichiometric with respect to the corresponding crystal, a surface crystallization tends to take place easily, because a nucleation at the surface of the glass sample occurs more easily than inside the glass sample. Such surface crystallized glasses have improved mechanical strength and often show non-linear optical behavior as well [25,26]. Optical micrograph of the surface crystallized glass ceramic ($Zn:Li:TeO_2$) sample is given in inset of Fig. 2.

3.3. UV–vis absorption

The absorption spectra of the crushed powdered glass and glass ceramic samples have been recorded in the range of 300–1100 nm (see Fig. 3). Effort has been made to keep the average particle size in the two samples nearly same in order to cancel out the effect of scattering. The UV absorption edge, which limits the transparency of the sample at shorter wavelength, is due to the absorption of the host matrix and is found to shift towards red region of visible spectrum on heating. The absorption spectra of these samples consist of nine absorption bands of Ho^{3+} ion at 362; 388; 419; 452; 475; 488; 539; 644; and 892 nm wavelengths corresponding to absorption from the ground state $^5I_8$ to the excited states $^3H_5 + {}^3H_6$; $^5G_4 + {}^3K_7$; $^5G_5$; $^5G_6 + {}^5F_1$; $^5F_2 + {}^3K_8$; $^5F_3$; $^5S_2 + {}^5F_4$; $^5F_5$; and $^5I_5$, respectively. It is clearly seen that the absorption peaks in ceramic samples are intense, narrower and more splitted compared to their glass counterparts. Furthermore, the peaks in $Zn:Li:TeO_2$ sample are almost two times intense compared to $Li:TeO_2$ ceramic sample. The observed variations reveal the changes in microenvironment around Ho^{3+} ions on heating.

The optical band gap has been calculated for the amorphous materials using the Mott and Davis relation [27]

$$\alpha h\nu = B(h\nu - E_g)^n$$

where B is band tailing parameter, E_g is the optical band gap, $n = 2$, 3, 1/2 and 1/3 corresponding to indirect allowed, indirect forbidden, direct allowed and direct forbidden transitions, respectively, and $h\nu$ is the incident photon energy. Band gap can be calculated from the linear region of the curve by extrapolating them to meet the $h\nu$ axis at $(\alpha h\nu)^n = 0$. Calculations reveal a slight reduction (3.7 eV) in the direct band gap of $Li:TeO_2$ glass ceramic sample compared to $Zn:Li:TeO_2$ glass ceramic sample (3.74 eV) (see Fig. 4).

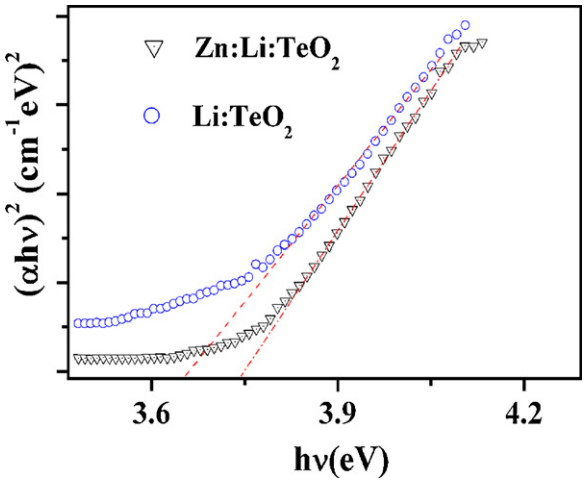

Fig. 4. Plot of $(\alpha h\nu)^2$ versus photon energy ($h\nu$) for direct band gap measurements of Li:TeO_2 and Zn:Li:TeO_2 glass ceramic samples.

3.4. FTIR analysis

The FTIR spectra of Li:TeO_2 and Zn:Li:TeO_2 glasses have been recorded and are shown in Fig. 5. As reported earlier, the addition of modifier modifies the tellurite glass structure by creating more non-bridging oxygen ions (NBOs) in the network [28]. For ZnF_2, which acts as network modifier, fluorine ion breaks up the continuous network and the divalent cation Zn^{2+} then produces non-bridging oxygen ions. As a result of the non-directed bonding to cations, the structural network collapses into closer packing and hence the density of network increases [29]. The NBOs created were believed to alter the glass structure in a way that packing of the molecules becomes denser as more network modifier ions attempt to occupy the interstices within the network. An increase of the density of the glasses accompanying the addition of ZnO probably changes the crosslink density and the coordination number of Te^{2+} ions [30].

As reported by earlier workers [31], the FTIR spectra for crystalline TeO_2 exhibit two absorption bands at 778 and 669 cm^{-1} which has been ascribed to the stretching vibration of equatorial and axial Te–O bonds in the TeO_4 units, respectively.

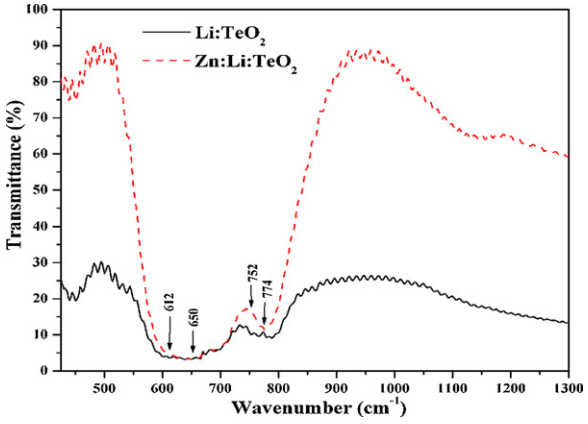

Fig. 5. Infrared absorption spectra of Li:TeO_2 and Zn:Li:TeO_2 glasses.

Previous studies [29] showed that Zn^{2+} enters into TeO_2 matrix. Evidence is the appearance of absorption peak positions shifting from 443 to 428 cm^{-1} with the increases in ZnO content.

The structure of TeO_2-based glasses is of interest because it contains two types of the basic structural units, i.e., TeO_4 trigonal bipyramid and TeO_3 trigonal pyramid. The IR vibrations at 425–463 cm^{-1} are attributed to the Te–O–Te chain unit symmetric stretching mode at corner sharing sites. The spectral features from 610 to 680 cm^{-1} and 750 cm^{-1} correspond to the TeO_4 bi-pyramidal arrangement and TeO_3 (and/or TeO_{3+1}) trigonal pyramids structures, respectively [32]. The presence of the modifier ions such as Zn^{2+} lead to the creation of TeO_3 and additional TeO_{3+1} polyhedra, which are responsible for the band at 779–790 cm^{-1} in all the tellurite glasses. The maximum phonon energy decreases and shifts from 788 cm^{-1} for Li:TeO_2 glass to 776 cm^{-1} for Zn:Li:TeO_2 glass.

3.5. Photoluminescence

3.5.1. Excitation with 532 nm laser

Up and downconversion emission spectra of Ho^{3+} doped Li:TeO_2 and Zn:Li:TeO_2 glass and glass ceramic samples were recorded with 532 nm laser excitation. Fig. 6 shows up and down-conversion emission spectra of Li:TeO_2 and Zn:Li:TeO_2 glass ceramic samples. The energy of 532 nm laser photon (~18,800 cm^{-1}) is not in resonance with any level of Ho^{3+} ion, however, the nearby energy levels $^5S_2$, $^5F_4$ lie at ~18,500 cm^{-1} energy and hence, only a weak phonon assisted absorption occurs. Due to this weak absorption, only down-conversion emission lines are observed from $^5S_2$, $^5F_4$ and $^5F_5$ levels up to 100 mW power of incident laser. The green emission from $^5S_2$, $^5F_4 \rightarrow {}^5I_8$ transition cannot be well resolved because it overlaps with the pump laser line, hence the region from 525 to 570 nm is not considered. A variation in red emission (661 nm) intensity of Ho^{3+} ion with its concentration is depicted in Fig. 7a. The emission intensity is found to be maximum for 1 mol.% concentration of Ho^{3+} ion. The emission intensity gets reduced for higher concentrations due to energy migration among Ho^{3+} ions.

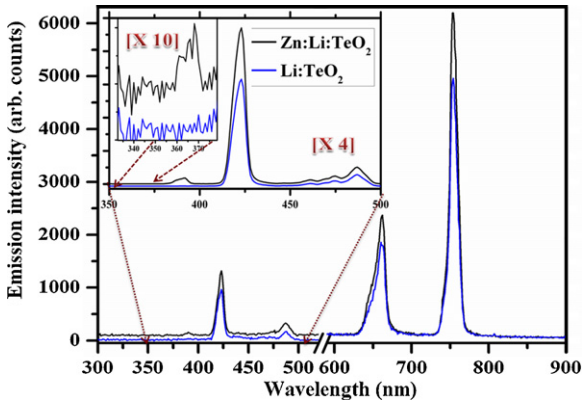

Fig. 6. Photoluminescence spectra of Li:TeO_2 and Zn:Li:TeO_2 glass ceramic samples with 532 nm laser excitation. An enlarged (4×) portion of the range 350–500 nm is given in inset.

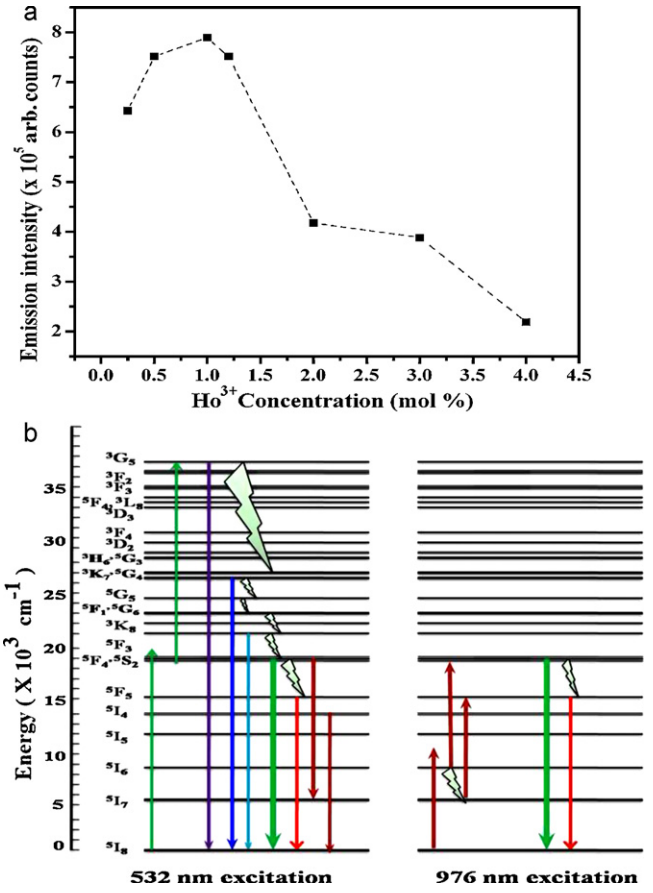

Fig. 7. Variation in red emission intensity of Ho^{3+} ions at different concentrations (a). Schematic energy level diagram of Ho^{3+} ions and the possible pathways of two photon absorption processes on excitation with 532 and 976 nm lasers (b).

As the laser power increases (>100 mW), several upconversion emission lines are observed in the range of 350–500 nm (inset of Fig. 6). In the presence of higher photon flux, the probability of two photon absorption is mostly anticipated, as the lifetime of the thermally coupled $^5S_2$, $^5F_4$ levels is found to be 150 μs.

During this course of time, the Ho^{3+} ions in the excited state reabsorb the incident 532 nm photons and promoted to $^3G_5$ level. The ions in $^3G_5$ level depopulate by emitting 420; 446; 461; and 469, 474, 486 nm wavelengths ascribed to $^3G_5$; $^5G_6$; $^5F_1$; and $^5F_3 + {}^5F_2 + {}^3K_8 \rightarrow {}^5I_8$ transitions, respectively, in Li:TeO_2 glass ceramic sample whereas no upconversion emission was observed in $LiTeO_2$ glass sample. Zn:Li:TeO_2 glass sample shows only a weak upconversion emission, while its glass ceramic sample shows improved upconversion emission intensities compared to Li:TeO_2 glass ceramic sample. Additionally, a few new weak peaks at 362, 365, 368; and 384 nm wavelengths ascribed to $^3H_5 + {}^5G_2 + {}^3H_6 + {}^5G_3 + {}^3L_9 + {}^3K_6 + {}^3F_4 + {}^3D_2$; and $^5G_4 + {}^3K_7 \rightarrow {}^5I_8$ transitions of Ho^{3+} ion, respectively, are also observed. The upconversion process in rare earth ions is the function of pump power, ion concentration, lifetime of the intermediate states etc. [33]. The downconversion bands observed at 660 and 754 nm are associated with the transitions $^5F_5 \rightarrow {}^5I_8$, and $^5S_2 \rightarrow {}^5I_7$ of Ho^{3+} ion, respectively.

The relationship between the emission intensity I_{em} and the NIR excitation intensity I_{ex} can be expressed as: $I_{em} = K(I_{ex})^n$ where K is a constant and n is the number of NIR photons absorbed per visible photon emitted. The fluorescence intensity for each spectral peak was represented by the integrated area under the corresponding spectral profile. A plot of log (I_{em}) versus log (I_{ex}) yields a straight line with a slope (n) = 1.95 for $^5G_5 \rightarrow {}^5I_8$ (384 nm) transition. On the basis of the power dependence and the observed emission lines, schematic energy level diagram is depicted in Fig. 7b.

3.5.2. Excitation with 976 nm laser

The photoluminescence spectra of the glass and glass ceramic samples of Li:TeO_2 and Zn:Li:TeO_2 were recorded in the 300–800 nm wavelength region under 976 nm diode laser excitation. All the glass samples show weak blue, intense green and red upconversion emissions; however, glass ceramic samples possess much better green upconversion emission intensity. (For interpretation of the references to color in text, the reader is referred to the web version of the article.) The green emission at 534 nm and 554 nm corresponds to $^5F_4$, $^5S_2 \rightarrow {}^5I_8$ transitions. The upconversion photoluminescence spectra show two red peaks centered at 665 and 751 nm, ascribed to $^5F_5 \rightarrow {}^5I_8$ and $^5F_4$, $^5S_2 \rightarrow {}^5I_7$ transitions, respectively. Emission at 751 nm is of particular interest as it is an excited to excited state transition which is suitable for development of lasers. The green upconversion emission intensity of the Zn:Li:TeO_2 glass ceramic is higher compared to Li:TeO_2 glass ceramic sample whereas red emission intensity in Zn:Li:TeO_2 glass ceramic is reduced considerably (see Fig. 8).

The upconversion mechanism of the aforesaid observations can be explained as follows: energy of 976 nm laser photon (~10,204 cm^{-1}) does not match with any energy level of Ho^{3+} ion. The closest energy level $^5I_6$ lies at ~8700 cm^{-1} which is 1549 cm^{-1} below the excitation wavelength. The $^5I_7$ level is metastable level and it acts as a good population reservoir allowing a high density of excited ions to be created. The absorption of incident photons by Ho^{3+} ions in $^5I_7$ level promotes ions to $^5F_4$, $^5S_2$ levels. The excited ions radiatively decay by emitting green and red photons corresponding to $^5F_4$, $^5S_2 \rightarrow {}^5I_8$ and $^5F_5 \rightarrow {}^5I_8$ transitions, respectively. Levels $^5F_4$

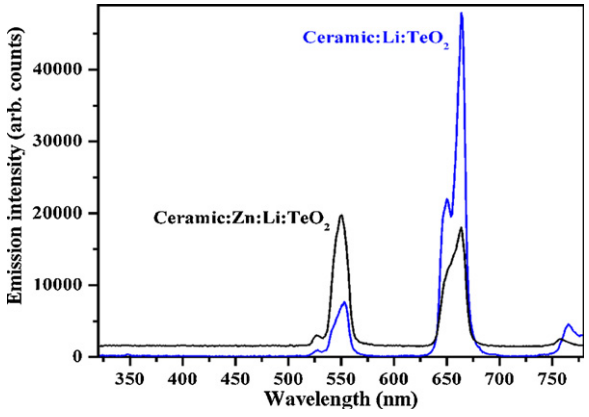

Fig. 8. Upconversion emission spectra of Li:TeO_2 and Zn:Li:TeO_2 glass ceramics on excitation with 976 nm laser radiation.

and $^5S_2$ are thermally coupled at room temperature and usually by taking aid of lattice vibrations, most of the ions relax through $^5S_2 \rightarrow {}^5I_8$ transition. In our case, the transition $^5S_2 \rightarrow {}^5I_8$ is stronger compared to $^5F_4 \rightarrow {}^5I_8$ transition.

The green to red peak ratio (I_{green}/I_{red}) in Li:TeO_2 and Zn:Li:TeO_2 ceramics is found to be 0.18 and 0.94, respectively. The drastic change in ratio is related to the comparatively lower vibrational environment of Ho^{3+} ions in Ho_2TeO_6 crystals, which efficiently hinders the nonradiative relaxation process from levels $^5F_4$, $^5S_2 \rightarrow {}^5F_5$, consequently, improves green emission from $^5F_4$, $^5S_2$ levels.

4. Conclusions

Structural and thermal properties of Li:TeO_2 and Zn:Li:-TeO_2 glasses and glass ceramics have been investigated using DTA, XRD and FTIR techniques. Besides the above properties, optical properties of these materials have also been made by the measurement of absorption, and emission (up and down-conversion) spectra. The up and downconversion emission spectra show different emission bands upon excitation with different laser wavelengths, i.e., with 532 and 976 nm. The XRD analysis shows the successful precipitation of two phases Ho_2TeO_6 and TeO_2 in major and minor proportions at much lower temperature in the presence of Zinc Fluoride that reveals its potential as catalyst.

Acknowledgements

Authors are thankful to Dr. R. N. Rai, Department of Chemistry, Banaras Hindu University, India, for providing UV–Vis absorption spectrophotometer. Mr. C. Joshi and Dr. Y. Dwivedi are thankful to the Council of Scientific and Industrial Research (CSIR), New Delhi, India for providing 'senior research fellowship'.

References

[1] G. Yi, H. Lu, S. Zhao, Y. Ge, W. Yang, D. Chen, L.H. Guo, Synthesis, characterization, and biological application of size-controlled nanocrystalline $NaYF_4$:Yb,Er infrared-to-visible up-conversion phosphors, Nano Lett. 4 (2004) 2191–2196.

[2] J.C Boyer, F. Vetrone, L.A. Cuccia, J.A. Capobianco, Synthesis of colloidal upconverting $NaYF_4$ nanocrystals doped with Er^{3+}, Yb^{3+} and Tm^{3+}, Yb^{3+} via thermal decomposition of lanthanide trifluoroacetate precursors, J. Am. Chem. Soc. 128 (2006) 7444–7445.

[3] A.S.G. Neto, L.A. Bueno, R.F. do Nascimento, E.A. da Silva Jr., E.B. da Costa, V.B. do Nascimento, White light generation by frequency upconversion in Tm^{3+}/Ho^{3+}/Yb^{3+}-codoped fluorolead germanate glass, Appl. Phys. Lett. 91 (2007) 091114-1–091114-3.

[4] L. Xie, Y. Wang, H. Zhang, Near-infrared quantum cutting in YPO_4:Yb^{3+}, Tm^{3+} via cooperative energy transfer, Appl. Phys. Lett. 94 (2009) 061905-1–061905-3.

[5] C. Li, N. Murase, Synthesis of highly luminescent glasses incorporating CdTe nanocrystals through sol-gel processing, Langmuir 20 (2004) 1–4.

[6] X. Qiao, X. Fan, J. Wang, M. Wang, Luminescence behavior of Er^{3+} ions in glass–ceramics containing CaF_2 nanocrystals, J. Non-Cryst. Solids 351 (2005) 357–363.

[7] A.S.G. Neto, E.B. da Costa, L.A. Bueno, S.J.L. Ribeiro, Upconversion luminescence in transparent glass ceramics containing β-PbF_2 nanocrystals doped with erbium, J. Alloys Compd. 375 (2004) 224–228.

[8] D. Chen, Y. Wang, Y. Yu, E. Ma, F. Bao, Z. Hu, Y. Cheng, Influences of Er^{3+} content on structure and upconversion emission of oxyfluoride glass ceramics containing CaF_2 nanocrystals, Mater. Chem. Phys. 95 (2006) 264–269.

[9] H. Ping, D. Chen, Y. Yu, Y. Wang, Judd–Ofelt analyses and luminescence of Er^{3+}/Yb^{3+} co-doped transparent glass ceramics containing $NaYF_4$ nanocrystals, J. Alloys Compd. 490 (2010) 74–77.

[10] J.A. Capobianco, J.C. Boyer, F. Vetrone, A. Speghini, M. Bettinelli, Optical Spectroscopy and upconversion studies of Ho^{3+}-doped bulk and nanocrystalline Y_2O_3, Chem. Mater. 14 (2002) 2915–2921.

[11] L. Feng, J. Wang, Q. Tang, L. Liang, H. Liang, Q. Su, Optical properties of Ho^{3+}-doped novel oxyfluoride glasses, J. Lumin. 124 (2007) 187–194.

[12] K. Kumar, S.B. Rai, D.K. Rai, Enhancement of luminescence properties in Er^{3+} doped TeO_2–Na_2O–PbX (X = O and F) ternary glasses, Spectrochim. Acta A 66 (2007) 1052–1057.

[13] A.M. Babu, B.C. Jamalaiah, J.S. Kumar, T. Sasikala, L.R. Moorthy, Spectroscopic and photoluminescence properties of Dy^{3+}-doped lead tungsten tellurite glasses for laser materials, J. Alloys Compd. 509 (2011) 457–462.

[14] O.V. Mazurin, M.V. Streltsina, T.P. Shvaiko-Shvaikovskaya, Handbook of Glass Data Part B, Elsevier, Amsterdam, 1985.

[15] S.H. Kim, T. Yoko, S. Sakka, Linear and nonlinear optical properties of TeO_2 glass, J. Am. Ceram. Soc. 76 (1993) 2486–2490.

[16] V. Dimitrov, T. Komatsu, Electronic polarizability, optical basicity and non-linear optical properties of oxide glasses, J. Non-Cryst. Solids 249 (1999) 160–179.

[17] S.I. Kim, S.I. Yun, Up-conversion in Pr^{3+}-doped tellurite glasses, J. Lumin. 60–61 (1994) 233–236.

[18] J.S. Wang, E.M. Vogel, E. Snitzer, Tellurite glass: a new candidate for fiber devices, Opt. Mater. 3 (1994) 187–203.

[19] H. Burger, W. Vogel, V. Kozhukharov, IR transmission and properties of glasses in the TeO_2–R_nO_m, R_nX_m, $R_n(SO_4)_m$, $R_n(PO_3)_m$ and B_2O_3] systems, Infrared Phys. 25 (1985) 395–409.

[20] J.E. Shelby, Introduction to Glass Science and Technology, RSC Publishing, UK, 2005.

[21] D.K. Durga, N. Veeraiah, Dielectric dispersion in ZnF_2–Bi_2O_3–TeO_2 glass system, J. Mater. Sci. 36 (2001) 5625–5632.

[22] M.M. Ahmed, C.A. Hogarth, M.N. Khan, A study of the electrical and optical properties of the GeO_2–TeO_2 glass system, J. Mater. Sci. 19 (1984) 4040–4044.

[23] M. Troemel, E. Munch, ICDD Grant-in-Aid, Institut fur Anorganische Chemie, Frankfurt, West Germany, 1989.

[24] S.F. Meier, T. Schleid, Crystal structure of dineodymium(III) hexaoxotellurate(VI), Nd_2TeO_6, Z. Kristallogr. NCS 219 (2004) 359–360.

[25] A. Narazaki, K. Tanaka, K. Hirao, Optical second-order nonlinearity of transparent glass-ceramics containing $BaTiO_3$ precipitated via surface crystallization, J. Mater. Res. 14 (1999) 3640–3646.

[26] Y. Dwivedi, S.B. Rai, Blue and red luminescence from europium-doped barium tetraborate crystals, J. Am. Ceram. Soc. 93 (2010) 727–731.

[27] N.F. Mott, E. Davis, Electronic Processes in Non-crystalline Materials, 2nd ed., Clarendon Press, Oxford, 1979.

[28] G.D. Khattak, M.A. Salim, X-ray photoelectron spectroscopic studies of zinc-tellurite glasses, J. Electron. Spectrosc. Relat. Phenom. 123 (2002) 47–55.

[29] H.A.A. Sidek, S.P. Chow, Z.A. Talib, S.A. Halim, Formation and elastic behavior of lead–magnesium chlorophosphate glasses, Turk. J. Phys. 28 (2004) 65–71.

[30] A.E. Adawy, Y. Moustafa, Elastic properties of bismuth borate glasses, J. Phys. D Appl. Phys. 32 (1999) 2791–2796.

[31] Y. Dimitriev, V. Dimitrov, M. Arnaudov, IR spectra and structures of tellurite glasses, J. Mater. Sci. 18 (1983) 1353–1358.

[32] R.A.E. Mallawany, Tellurite Glass Handbook, CRC Press, New York, 2002.

[33] Y. Dwivedi, A. Rai, S.B. Rai, Intense white upconversion emission in Pr/Er/Yb codoped tellurite glass, J. Appl. Phys. 104 (2008) 043509-1–043509-4.